JOURNAL OF MATERIALS SCIENCE 39 (2004) 4799 – 4807

Mechanical and thermal properties of physical vapour deposited alumina films

Part I *Thermal stability*

J. THURN*, R. F. COOK‡
Department of Chemical Engineering and Materials Science, University of Minnesota, Minneapolis, MN 55455, USA
E-mail: rfc@cems.umn.edu

Thermal stability of non-reactive physical vapour deposited alumina films of varying thickness on Al_2O_3-TiC and Si substrates, deposited at two different substrate biases, is examined. Substrate curvature measurements were used to determine the deposition stress and stress development during thermal cycling and annealing. Thermal cycling experiments revealed that the films deposited on Al_2O_3-TiC substrates become irreversibly more compressive on heating and annealing while films deposited on Si substrates become irreversibly more tensile. The deposition stress was found to be independent of film thickness, substrate material, and substrate bias during deposition. The thermal stability was independent of film thickness and substrate bias during deposition.
© *2004 Kluwer Academic Publishers*

1. Introduction

Physical vapour deposited (PVD) alumina films are used in many applications, including passivation in metal oxide semiconductor devices [1], as electrically insulating coatings [2–4], as optical coatings [5, 6], and as basecoats and protective overcoats on magnetic recording heads [7, 8]. The basecoats and overcoats for insulation and encapsulation of magnetic recording heads are relatively thick films, about 5 and 40 μm, respectively, and are typically deposited from polycrystalline Al_2O_3 sputter sources (non-reactive PVD). The basecoat is applied directly to an Al_2O_3-TiC ceramic composite substrate and provides the foundation for the remainder of the recording head films, while the overcoat encapsulates the entire recording head. Adhesion of the basecoat to the substrate is obviously a prime concern, as the entire head is built on the basecoat. The overcoat encapsulation serves to protect the recording head and should be stiff and fracture-resistant. Furthermore, stress in the alumina films, arising during deposition or from coefficient of thermal expansion (CTE) mis-match with the substrate ("thermal stress"), can have a profound effect on the magnetic behaviour of the metal films in the recording head stack. If these deposition or thermal stresses cannot be predicted, and then accounted for in the production of the rest of the head, the magnetic performance and mechanical reliability of the head comes into question. Prediction and optimisation of the mechanical behaviour of recording heads thus relies on detailed knowledge of the elastic and plastic properties of the films in question. As a consequence, characterization of alumina films for magnetic recording head applications should include techniques to measure the film's stress development and adhesion, elastic, plastic, and fracture properties.

Many studies characterizing non-reactive PVD alumina films have been carried out. It has been found that films deposited by physical vapour techniques often display variations in structure and mechanical and optical properties on changes in the deposition conditions [1, 4, 6–11]. The complicated way in which variations in input power, substrate bias voltage, chamber pressure, and substrate temperature have affected the mechanical properties of the deposited film has precluded *a priori* predictions of such properties, and thus each film has been characterized individually or as a function of a single processing parameter. There are, however, some overall statements that may be made about PVD alumina films. First, films deposited from alumina targets (non-reactive PVD) are amorphous in character [1, 4, 9, 10, 12, 13]. Second, incorporation of Ar (a sputtering gas) in the film during the deposition process results in a compressive film stress, which subsequently increases in magnitude on annealing or thermal cycling [9]. The incorporation of Ar is thought also to decrease the modulus from that of bulk polycrystalline Al_2O_3 [11]. Third, the films may or may not be stoichiometric [1, 4, 8–10], and hence will be referred to as AlO_x in this study.

**Present address:* Advanced Mechanical Technology, Mechanical Research and Development, Seagate Technology, Bloomington, MN 55435, USA.
‡Author to whom all correspondence should be addressed.

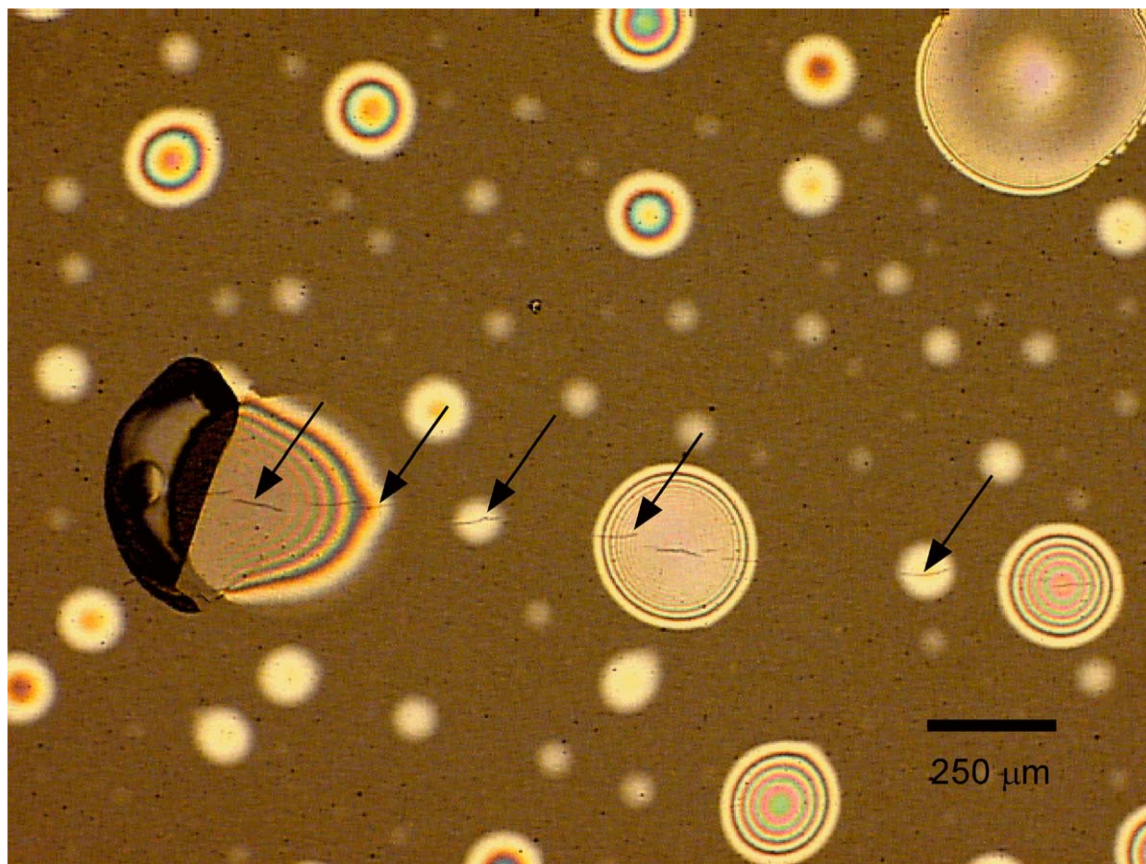

Figure 1 A 16 μm AlO_x film (on Al_2O_3-TiC substrate) exhibiting debonding, through-film cracking, and chipping, following thermal cycling to 800°C. Debonding is circular and can be identified by interference fringes and through-film cracking is identified with arrows.

The purpose of this work is to examine the adhesion, fracture, elastic, plastic, and thermo-mechanical properties of PVD alumina films of varying thicknesses deposited at two different substrate biases, with all other deposition conditions held constant. Film stress is examined using a substrate curvature measurement instrument capable of measuring the curvature during heating and cooling. The stress responses of the various film-substrate systems to thermal cycling and annealing are compared. Non-equilibrium stress development during thermal cycling and annealing is related to film mechanical properties. Fig. 1 shows a 16 μm AlO_x film following thermal cycling to 800°C. Circular debonds—evident as the circular interference fringes—range in diameter from 40 to 470 μm. Also evident are chipping and film cracking. Chipping occurred at the edges of some debonds and film cracking (identified with arrows in Fig. 1) occurred in both the debonded and adhered regions of the film. The features of Fig. 1 highlight three properties of AlO_x films that will be examined in this paper and the accompanying part II: (i) the films become more compressive during heating; (ii) the films exhibit both through-film cracking and interfacial cracking (debonds), implying that the film and interfacial fracture resistances are of the same magnitude; and (iii) the fracture and deformation is confined to the film—the substrate did not chip or crack while the film debonded, cracked, or chipped completely off the substrate. The focus here in part I is on the thermo-mechanical stability of the AlO_x film, as characterized by film stress variations.

2. Analysis

Substrate curvature measurements were used to calculate changes in equi-biaxial film stress using Stoney's approximation [14]:

$$\Delta\sigma_f = \Delta\kappa \frac{E_s t_s^2}{6(1-\nu_s)t_f}, \quad (1)$$

where $\Delta\sigma_f$ is the change in film stress associated with a measured change in substrate curvature $\Delta\kappa$. E_s is the substrate modulus, ν_s is the substrate Poisson's ratio, t_s is the substrate thickness, and t_f is the film thickness. The measured change in curvature was due to either film deposition or a change in temperature. Thermal stress development can be related to the CTE mismatch between the film and substrate using the thin film approximation:

$$\Delta\sigma_f = \frac{E_f}{1-\nu_f}(\alpha_s - \alpha_f)\Delta T, \quad (2)$$

where E_f and ν_f are the film modulus and Poisson's ratio, respectively, α_i are the CTE, and ΔT is a change in temperature. Equation 2 can be used to determine the film CTE (provided the film modulus and substrate CTE are known) from a measured linear elastic stress-temperature slope. The substrate properties used in this study were: $E_s = 420$ GPa, $\nu_s = 0.2$ (assumed), $\alpha_s = 7.8$ ppm K^{-1} for Al_2O_3-TiC [15], and $E_s = 168.9$ GPa, $\nu_s = 0.068$ [16], and $\alpha_s = 2.9$ ppm K^{-1} (measured with a dilatometer) for (100) Si.

The slope of an assumed linear thermal stress-temperature response contains information about the modulus of the film and the CTE mis-match between the film and the substrate (Equation 2). If a film is deposited on two different substrates and the CTE of both substrates known, then the slopes of the different thermal stress responses can be used to determine the biaxial modulus and CTE of the film, known as the "double-substrate method" [17]. The differentiatial form of Equation 2 is:

$$\frac{d\sigma_f}{dT} = E_f^+(\alpha_s - \alpha_f), \tag{3}$$

where $E_f^+ = E_f/(1 - \nu_f)$ is the film biaxial modulus. If Equation 3 is written for thermal stress development for AlO_x films on both Al_2O_3-TiC and Si substrates, the biaxial modulus and CTE of the film are:

$$E_f^+ = \frac{\frac{d\sigma_f}{dT}\big|_{Al_2O_3\text{-TiC}} - \frac{d\sigma_f}{dT}\big|_{Si}}{\alpha_{Al_2O_3\text{-TiC}} - \alpha_{Si}} \tag{4}$$

and

$$\alpha_f = \frac{\alpha_{Si}\,\frac{d\sigma_f}{dT}\big|_{Al_2O_3\text{-TiC}} - \alpha_{Al_2O_3\text{-TiC}}\,\frac{d\sigma_f}{dT}\big|_{Si}}{\frac{d\sigma_f}{dT}\big|_{Al_2O_3\text{-TiC}} - \frac{d\sigma_f}{dT}\big|_{Si}}. \tag{5}$$

For this method to work, the film should be identical on both substrates so that only the CTE of the substrate affects the thermal stress response.

3. Experimental procedure

Alumina films were deposited by non-reactive r.f. diode sputtering from a sintered Al_2O_3 target onto polished ceramic polycrystalline Al_2O_3-TiC (64 Al_2O_3 − 35 TiC − 1 additives wt%) and (100) Si substrates, with −50 V and −130 V substrate biases. The substrate was at approximately 50°C during deposition. The films ranged in thickness from 2.5 to 50 μm, the Al_2O_3-TiC substrates were 115 mm square and 2 mm thick, and the (100) Si wafers were 500 μm thick and 100 mm in diameter. Film thicknesses were determined from calibrated deposition rates and confirmed by profilometry. Table I identifies the specimen naming scheme used in this study. (Films deposited at a 'high' bias of −130 V are designated 'AH' and films deposited at a 'low' bias of −50 V are designated 'AL.') The Al_2O_3-TiC substrates had an average grain size of 0.5–1.5 μm and a density of 4.3 g cm^{-3} [15].

Substrate curvature was measured using a commercial tool (FSM 900TC Frontier Semiconductor, Inc., San Jose, CA), that uses an optical lever technique with a 750 nm He-Ne laser. The sample chamber was evacuated to at least 10^{-3} torr, heated at 5°C min^{-1}, and cooled at the same rate except under 100°C, when cooling was exponential. For more details, see [18] or [19]. Platinum films 120 nm thick were deposited on the substrate by d.c. sputtering (opposite the alumina film) to improve the reflectivity. During thermal cycling, five curvature measurements were taken every 25°C after holding at a temperature for 2 min. Each biaxial film stress measurement was determined from curvatures measured in four orientations across the sample (45° apart). The samples were cycled three times to peak temperatures ranging from 100 to 500°C (in increments of 100°C). The films were examined optically following the cycles to each peak temperature for evidence of cracking, delamination, or buckling.

A significant source of uncertainty of the biaxial stress measurements arose from the curvature measurement resolution. Relatively thin films on thick substrates caused little substrate curvature change on deposition and with changes in temperature. The maximum detectible changes in radius of curvature was on the order of 1 km; any changes in radius of curvature greater than this lead to significant stress uncertainty (on the order of 1–10 MPa).

The composition of selected films was determined before and after thermal cycling using Rutherford Back Scattering (RBS) with 2 MeV He$^+$ ions. Normal incidence and 165° backscattering angles were used and the maximum penetration depth was about 2–2.5 μm.

TABLE I AlO_x film deposition and thermal cycling parameters

				Thermal cycling		
Specimen ID	Substrate bias (V)	Film thickness (μm)	Deposition stress (MPa)	Peak temp. (°C)	Athermal stress hysteresis (MPa)	Thermal stress development (MPa K^{-1})
AH1	−130	47.9 ± 3.8	−50 ± 5	100	−3 ± 1	0.031 ± 0.004
				200	−18 ± 1	0.047 ± 0.002
				300	−62 ± 1	0.062 ± 0.005
				400	−126 ± 1	0.078 ± 0.003
				500	−178 ± 1	0.085 ± 0.002
AH2	−130	46.0 ± 0.6	–	300	−63 ± 1	0.049 ± 0.001
AH3	−130	16 ± 0.2	–	–	–	–
AH4	−130	12 ± 0.2	−41 ± 5	300	−76 ± 8	0.077 ± 0.003
AH5	−130	7.3 ± 0.1	–	300	−87 ± 10	0.142 ± 0.008
AH6	−130	7.3 ± 0.1	–	–	–	–
Si1	−130	2.5 ± 0.1	−46 ± 2	300	+24 ± 2	−0.494 ± 0.007
AL1	−50	16 ± 0.2	–	–	–	–
AL2	−50	16 ± 0.2	–	300	−72 ± 4	0.161 ± 0.007
AL3	−50	12 ± 0.2	−37 ± 11	300	−69 ± 8	0.148 ± 0.004
AL4	−50	7.3 ± 0.1	–	300	−88 ± 7	0.184 ± 0.018

4. Results and discussion

4.1. Room temperature deposition stress

The room temperature deposition stress was measured on three films deposited on Al_2O_3-TiC substrates, as shown in Table I. Two of the films, AH1 and AH4, were deposited at the same substrate bias of −130 V but had different thicknesses. The measured compressive deposition stresses of -50 ± 5 and -41 ± 5 MPa for these 50 and 12 μm films, respectively, were within experimental uncertainty of each other, indicating the deposition stress was independent of film thickness, in agreement with Christova and Szekeres [12]. The third film, AL3, was 12 μm thick deposited at a substrate bias of −50 V and had a deposition stress of -37 ± 11 MPa, also within experimental uncertainty of the −130 V films. The magnitude of the deposition stresses were similar in sign and magnitude to those obtained by other researchers [7, 11, 12]. The deposition stress of Si1, a 2.5 μm film on Si (−130 V), was measured to be -46 ± 2 MPa, the same as the deposition stresses measured for films on Al_2O_3-TiC. Within experimental uncertainty, deposition stress was not sensitive to substrate bias, substrate material, or film thickness.

4.2. Thermal and athermal stress development

Eight films were thermally cycled to peak temperatures of up to 500°C as outlined in Section 3 and noted in Table I. The thermal stability plot for AH1 is shown in Fig. 2. Deposited in 50 ± 5 MPa of compression, the film was cycled to peak temperatures of 100 to 500°C, at least three times to each peak temperature. Stress measurements taken on heating are shown as solid symbols and measurements taken on cooling as open symbols; the uncertainty associated with each stress measurement is approximately the symbol size (on the order of 1 MPa). The stress development on thermal cycling was similar to that observed previously for dielectric films [19]: a nonlinear hysteretic stress development on the first cycle to a given peak temperature, followed by nearly linear thermal-stress development due to CTE mis-match on subsequent cycles to that temperature. The nonlinear hysteretic stress development was not a result of CTE mis-match between the film and substrate, and is termed "athermal" stress. In previously examined cases of stress hysteresis on thermal cycling in plasma-enhanced chemical vapour deposited (PECVD) [19, 20], spin-on deposited (SOD) [21, 22], and ion-beam assisted deposited (IBAD) [23] dielectric films, the irreversible stress development was tensile, whereas the PVD AlO_x films examined here became more compressive, consistent with previous experiments on free-standing PVD alumina films [9]. The slope of the thermal stress response to each peak temperature was positive (film stress change was tensile on heating) indicating that the film CTE was less than that of the Al_2O_3-TiC substrate. The slope increased on cycling to increasing peak temperatures and this can be attributed to either a decrease in film CTE (already smaller than that of the Al_2O_3-TiC substrate) or an increase in the film modulus (Equation 2). These changes in film properties (CTE and/or modulus) can be associated with impurity diffusion, plastic deformation, or structural rearrangement accompanying the stress hysteresis on the first cycle to a given peak temperature.

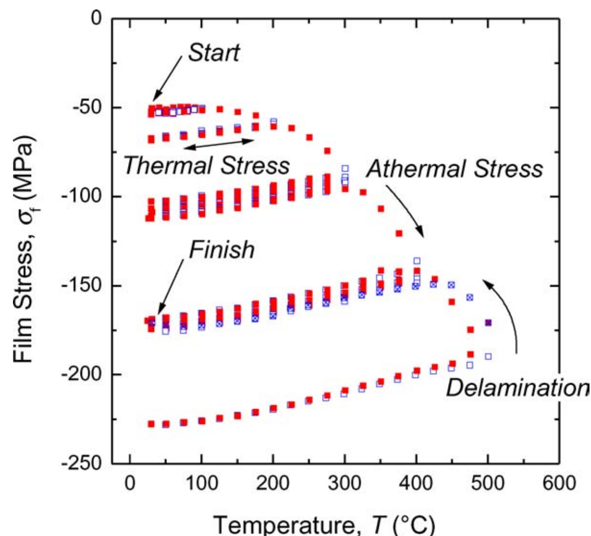

Figure 2 Stress development in ∼50 μm AlO_x film AH1 on thermal cycling to peak temperatures of 100 to 500°C. The initial heating cycle to each peak temperature resulted in nonlinear, irreversible stress development. Stress variation on subsequent cycles were nearly linear, due to CTE mis-match between the film and substrate. (Heating cycles are solid squares and cooling cycles are open squares.) The film partially delaminated due to excessive compressive film stress during the final cooling cycle (shown as open squares with crosses through them).

The amount of hysteretic stress development increased with each increment in peak temperature and was confined primarily to the heating half of the first cycle. The amount of stress hysteresis was 3 ± 1 MPa (compressive) on the first heating cycle to 100°C but increased to ∼60 MPa on the first cycles to 400 and 500°C. Table I shows the cumulative room temperature difference from deposition stress following cycles to each peak temperature for AH1. There were only two cycles performed at the 500°C peak temperature. The first heating cycle, as mentioned above, resulted in 52 ± 1 MPa of incremental compressive athermal stress development while the first cooling cycle was approximately linear. Subsequent heating resulted in stress development indistinguishable from the previous cooling cycle, as expected for thermal stress development due to CTE mis-match. However, the second cooling cycle saw an apparent nonlinear *decrease* in film stress near 500°C followed by erratic stress development on further cooling to room temperature. (The stress data from this cooling cycle are shown in Fig. 2 as crossed open symbols.) The apparent film stress following this cooling cycle was about 50 MPa *less* compressive than the film stress at room temperature following the previous cooling cycle. Inspection of the sample following these two cycles to 500°C revealed that approximately half of the film had fully delaminated. Presumably the magnitude of compressive stress developed on cycling to 500°C, particularly during the first cooling cycle to room temperature, provided the driving force for film delamination and further cycling exacerbated the effect. The decrease in film stress due to film delamination was

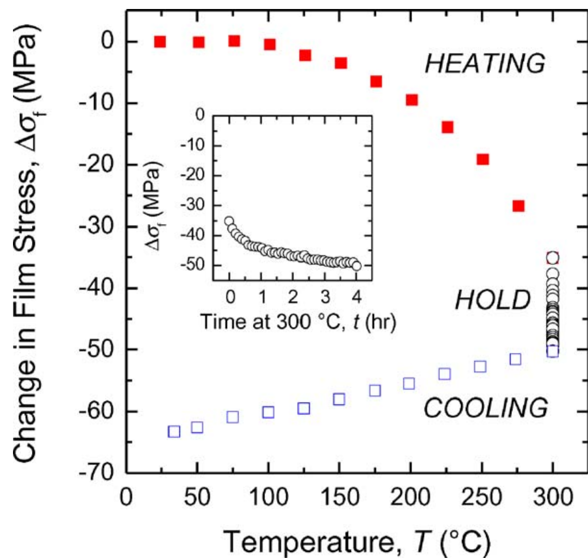

Figure 3 Stress development in ~50 μm AlO_x film AH2 on thermal cycling with a four-hour anneal at the peak temperature of 300°C. The inset shows stress development with time during the anneal.

approximately the same magnitude as the deposition stress reported in Table I, suggesting that delamination almost completely deconstrained the substrate.

A second ~50 μm film, AH2, was not thermally cycled but rather annealed at 300°C for four hours. As shown in Fig. 3, the majority of nonlinear stress development occurred during the heating cycle. (The ordinate of Fig. 3 is "change in biaxial film stress," as the deposition stress of this particular film was not measured—it can be assumed to be on the order of −50 MPa—and the uncertainty in stress is again the symbol size.) Further stress development occurred during the anneal, shown as open circles in Fig. 3. The cooling cycle saw linear thermal stress development due to CTE mis-match. The time dependence of the stress development during the anneal is shown in the inset of Fig. 3. The stress became more compressive in an approximately exponential manner, with 80% of the stress developing during the first two hours of the anneal. The total change in stress (from 0 at room temperature on deposition to the final measured stress at room temperature following the cooling cycle) during the thermal excursion was −63 ± 1 MPa, as shown in Table I. This can be compared with the change in stress following thermal cycling to 300°C of AH1, also shown in Table I, to be −62 ± 1 MPa. The net change in room temperature film stress was the same, whether the film was cycled to peak temperatures of 100, 200, then 300°C multiple times, or annealed at 300°C for four hours.

Two other films of different thicknesses were deposited on Al_2O_3-TiC substrates at biases of −130 V: AH4 (12 μm) and AH5 (7.2 μm). These films were thermally cycled to peak temperatures of 100, 200, and 300°C; twice to each peak temperature with a three hour anneal at 300°C on the first excursion to that temperature. Fig. 4a–c show the thermal stability plots for AH2, AH4, and AH5. The ordinate scale for all three figures is the same (change in stress from the room temperature deposition stress) for a clear comparison of the hysteresis behaviour on thermal cycling. The thermal stability plots are similar in character to Fig. 2 but with greater stress uncertainty of about 8 and 10 MPa for the 12 and 7.2 μm films, respectively. (The increase in uncertainty is due to decreased film thickness and thus decreased changes in substrate curvature for a given change in temperature.) Both films had somewhat greater athermal stress development following the heat treatment than films AH1 or AH2 (Table I and Fig. 4). This is probably due to their heat treatment combining the effects of both thermal cycling to multiple peak temperatures and an anneal at 300°C. To within ±20% the magnitude of athermal stress development during the heat treatment to 300°C, like the deposition stress, was independent of film thickness for films deposited at a substrate bias of −130 V.

One film (Si1) was deposited at a bias of −130 V on a (100) Si substrate and subjected to the same heat treatment as AH4 and AH5. The stress development during thermal cycling and annealing is shown in Fig. 5. Three points are immediately evident from Fig. 5: (i) the room temperature deposition stress, as noted previously, is approximately the same as for AlO_x films on Al_2O_3-TiC substrates; (ii) the slope of the thermal stress response is negative, opposite that of AlO_x films on Al_2O_3-TiC substrates and implying the film CTE is greater than that of Si; and (iii) there is no hysteresis on cycling to 100 and 200°C and the film stress

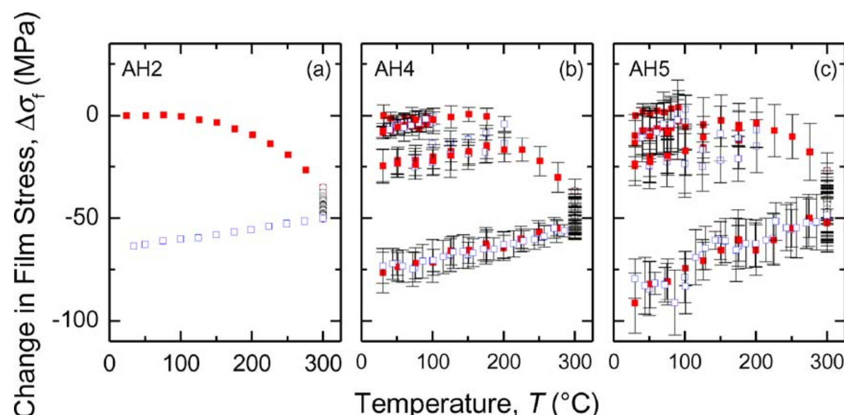

Figure 4 Thermal stability plot of (a) AH2, (b) AH4, and (c) AH5. The ordinate scales are the same on all three plots. The room temperature deposition stress has been arbitrarily set to zero for all three films. AH2 was annealed for four hours at 300°C while AH4 and AH5 were thermally cycled to peak temperatures of 100 and 200°C prior to a three-hour anneal at 300°C.

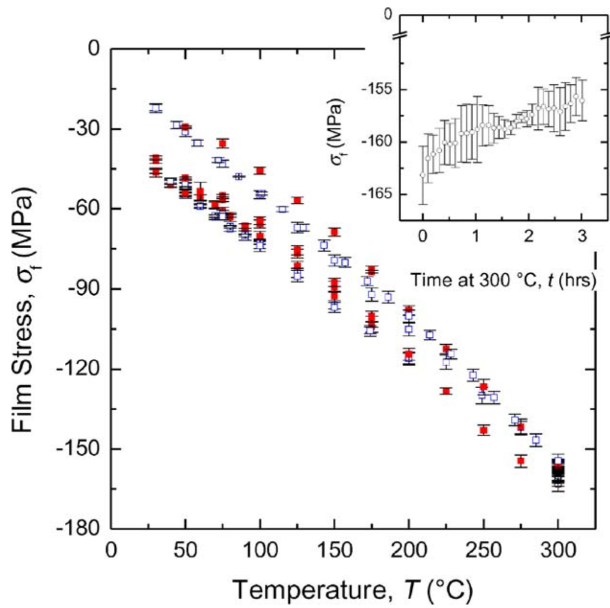

Figure 5 Stress development in Si1 on thermal cycling to peak temperatures of 100, 200, and 300°C with a three hour anneal at 300°C during the first cycle to that temperature. The inset shows stress development with time during the anneal.

becomes somewhat more tensile during annealing at 300°C, again opposite that of AlO_x films on Al_2O_3-TiC substrates. The second point places limits on the film CTE: 2.9 ppm $K^{-1} < \alpha_f < 7.8$ ppm K^{-1}. The third point suggests that AlO_x responds to thermal loading differently when deposited on different substrates.

The double-substrate method was used to extract the biaxial modulus and CTE of the AlO_x film from Si1 and AH4 (both deposited at a substrate bias of −130 V). The thermal stress responses of both systems following the 300°C anneal were used to estimate $E_f^+ = 117 \pm 4$ GPa and $\alpha_f = 7.1 \pm 0.3$ ppm K^{-1} (Equations 4 and 5). If ν_f is assumed to be 0.2 (for a glassy material) then $E_f = 93 \pm 3$ GPa.

As noted in Table I, three AlO_x films of different thicknesses were deposited on Al_2O_3-TiC substrates at a bias of −50 V. All three were subjected to the same heat treatment as AH4 and AH5. The thermal stability plots of all three are shown in Fig. 6a–c. Nonlinear compressive athermal stress developed on the first cycle to a given peak temperature and the magnitude of

TABLE II AlO_x film compositions

Film	Composition (at.%) Ar	Al	O	Al/O	Atomic density (at. $cm^{-3} \times 10^{22}$)
AH5 as deposited	6.0 ± 0.4	38.5	55.5	0.69	6.45
AH5 annealed at 300°C	6.0 ± 0.4	39.1	54.9	0.71	6.42
AL4 as deposited	5.2 ± 0.3	40	54.8	0.73	6.45
AL4 annealed at 300°C	5.2 ± 0.3	40	54.8	0.73	6.45

the athermal stress increased with increasing peak temperature. Subsequent cycles to a given peak temperature resulted in thermal stress development due to CTE mis-match between the film and substrate. This thermal stress response was positive and increased slightly with increasing peak temperature. The compressive stress development during the anneal at 300°C was, as before, approximately exponential. The magnitude and sign of stress hysteresis, as determined by the difference in room temperature stress values before and after the heat treatments, were the same as for films deposited at a substrate bias of −130 V (Table I).

RBS was used to determined the composition of films AH5 and AL4 before and after thermal cycling to 300°C: Table II gives the estimated Al, O and Ar contents and atomic density. Films deposited at both high and low bias had substantial included Ar fractions (5–6 at%) that were not removed on thermal cycling and annealing to 300°C, consistent with the observations of Gardner *et al.* [9]. Both films were also somewhat Al rich relative to stoichiometric, crystalline, Al_2O_3 (Al/O of 0.67), also consistent with the observations of Gardner *et al.* [9], and exhibited smaller atomic density relative to crystalline Al_2O_3 (1.18×10^{23} at. cm^{-3}).

5. Discussion

The observation here, that deposition stress (the stress observed at room temperature immediately after deposition) in non-reactively sputtered AlO_x films was invariant with film thickness, substrate bias or substrate type, is of great practical importance. Process windows may be made large and films incorporated in different stacks with confidence that the deposition stress will not be too much affected. In addition, the level of stress

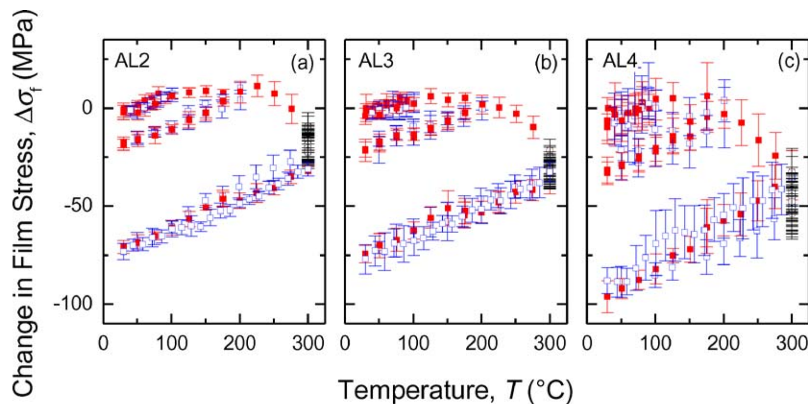

Figure 6 Thermal stability plot of (a) AL2, (b) AL3, and (c) AL4. The ordinate scales are the same on all three plots. The room temperature deposition stress has been arbitrarily set to zero for all three films. The films were thermally cycled to peak temperatures of 100 and 200°C followed by a three-hour anneal at 300°C.

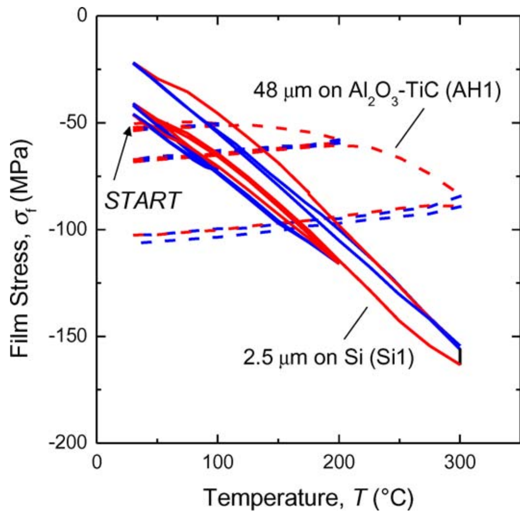

Figure 7 Stress development in AlO_x films deposited on AlTiC and Si substrates thermally cycled to 300°C. The film on AlTiC exhibited very small, reversible tensile thermal stress change and large, irreversible compressive stress development on cycling. The film on Si exhibited large, reversible compressive thermal stress change and very small tensile stress development.

hysteresis (the irreversible change in stress observed at room temperature after cycling to and from a greater temperature) was observed to be independent of film thickness and substrate bias, suggesting that changes in stress on subsequent thermal cycling will also not depend too much on deposition conditions.

This last point, however, must be tempered with the observation that the nature and degree of stress hysteresis was dependent on substrate *type*. Fig. 7 is a composite plot of the stress development in systems AH1 and Si1 on thermal cycling up to 300°C; the films were deposited under identical conditions onto Al_2O_3-TiC and Si substrates, respectively. The film on the Si substrate exhibited small, tensile, stress hysteresis on thermal cycling while the film on the Al_2O_3-TiC substrate exhibited large, compressive, stress hysteresis. As the observations above suggest that the nature of the substrate only influences the stress in the film through CTE mismatch effects, the implication is that athermal stress development in these AlO_x films depends on the total stress level. This is of practical importance, of course, as it suggests that changes in film stress on thermal cycling will depend on substrate type through more than direct CTE effects, but, in addition, points to factors controlling the underlying structure of the films.

In developing an explanation for the differing stress hysteresis behaviors of films on different substrates (and thus experiencing different stress states), we note some of the observations by Gardner *et al.* [9] of stress-free AlO_x films removed from their substrates and thermally cycled. These free-standing films exhibited hysteretic tensile strains with no change in composition on thermal cycling up to 800°C, with the magnitude of the stress-free strain hysteresis increasing with increasing peak temperature. (For peak temperatures greater than about 840–865°C, Ar was observed to evolve from the film and the hysteresis strain became compressive.) Gardner *et al.* rationalized these observations by comparison with the behavior of inert gases trapped or dissolved in irradiated metals: On thermal cycling or annealing below 840–865°C, Ar incorporated during the sputter-deposition of the films coalesces into bubbles or voids leading to irreversible constraint- and stress-free swelling of the film. The irreversible *compressive* stress development observed here during thermal cycling and annealing of similar films on Al_2O_3-TiC substrates is then explained by the constraint of the substrate on the imposed *tensile* strain associated with Ar exsolution, coalescence and void formation. The lack of observed similar stress development in films on Si substrates can be explained by extending this idea to include the effects of stress on the solubility of Ar in the AlO_x structure.

The pressure dependence of the equilibrium concentration of a *dissolved* gaseous species in a solid is given by [24]

$$X_i = X_{i0} \exp\left(\frac{-p\Delta\bar{V}_i}{RT}\right), \tag{6}$$

where X_i is the equilibrium concentration, p is the pressure, $\Delta\bar{V}_i$ is the change in the partial molar volume of the species on dissolution, T is temperature and R is the universal gas constant. For positive pressure (a compressive stress), $p > 0$, and $\Delta\bar{V}_i < 0$ (dissolved impurities occupy less volume than exsolved) the equilibrium dissolution concentration is greater than the zero pressure value, X_{i0}. The combined observations of AlO_x films on no substrate, Al_2O_3-TiC substrates, and Si substrates may then all be interpreted via Equation 6 in terms of progressively increased levels of compressive stress leading to increased equilibrium levels of Ar incorporation or dissolution, and thus decreased tendency for Ar coalescence and associated void formation and swelling during heat treatment. We consider here the simplified case of all three systems rapidly heated to 300°C, annealed for a long time and then rapidly quenched, as shown in the schematic time-temperature inset diagram of Fig. 8.

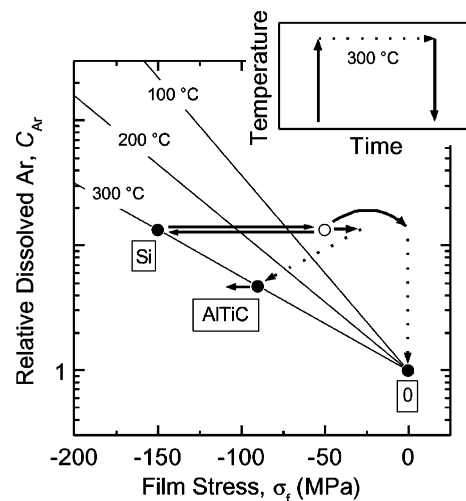

Figure 8 Schematic stress-concentration indicator diagram with equilibrium dissolution concentration isotherms drawn. Equilibrium concentrations for 300°C anneals at various stress levels are indicated by solid symbols and the initial deposition condition of an Ar-containing AlO_x film indicated by the open symbol. The behaviour of the film on various substrates during an anneal (inset) is indicated by the solid and dashed lines.

Fig. 8 is a schematic stress-concentration indicator diagram showing the isotherms from Equation 6, identifying the film stress $\sigma_f = -p$ and the equilibrium concentration of dissolved Ar relative to the zero stress value as $C_{Ar} = X_i/X_{i0}$. *Equilibrium* stress-concentration points on the 300°C isotherm appropriate to no substrate (0), an Al_2O_3-TiC substrate (AlTiC) and a silicon (Si) substrate are indicated as solid symbols. A just-deposited AlO_x film is in a non-equilibrium state, with a value of C_{Ar} too large for the small compressive stress level associated with deposition and cooling to room temperature. This initial state is indicated on the diagram by the open symbol and is taken to be common for all three cases to be considered. On removal of the substrate (as in the experiments of Gardner *et al.*) the film becomes stress-free (with a small lateral expansion). This (rapid) perturbation process is indicated on the diagram by the solid curved line. On subsequent isothermal annealing (indicated schematically in the inset), the film approaches equilibrium by "precipitating" Ar out of solution into voids, with consequent free expansion. This (slow) irreversible process is indicated on the diagram by a dashed vertical line. Eventually the dissolved Ar concentration reaches the equilibrium value of $C_{Ar} = 1$ appropriate to $T = 300$°C and $\sigma_f = 0$ and the exsolution, void formation and expansion processes halt. This final equilibrium state is indicated by the boxed symbol 0. On (rapid) cooling to room temperature the film remains metastably trapped in this state. Fig. 9a shows a schematic representation of this constraint-free process.

At the other extreme is the behavior of the maximally constrained film annealed on a Si substrate, also indicated in Fig. 8 and represented in Fig. 9c. On rapid heating of this system from the initial, common, room temperature state (open symbol), the film is placed in significant compression due to the positive CTE mismatch with the Si substrate, again indicated on the diagram by a solid (horizontal) line. This perturbation places the film at a relative concentration level approximately on the equilibrium isotherm and now on subsequent isothermal annealing the film remains close to equilibrium, with consequent little imposed deformation. The lack of imposed deformation leads to essentially no stress development at $T = 300$°C and $\sigma_f \sim -150$ MPa. On (rapid) cooling to room temperature from this state the compressive stress associated with the CTE mismatch reverses (indicated by another horizontal solid line) and the film remains metastably trapped in the high temperature state, which is indicated on the diagram by the boxed symbol Si.

The final, intermediate, case is that of the film annealed on an Al_2O_3-TiC substrate, also indicated in Fig. 8 and represented in Fig. 9b. On rapid heating of this system from the initial state, the film is placed in a slightly less compressive stress due to the small negative CTE mismatch with the Si substrate, indicated on the diagram by a short (horizontal) solid line. This perturbation places the film at a relative dissolved Ar concentration level greater than the equilibrium isotherm, similar to that for the substrate-free case, and again on subsequent isothermal annealing the film approaches

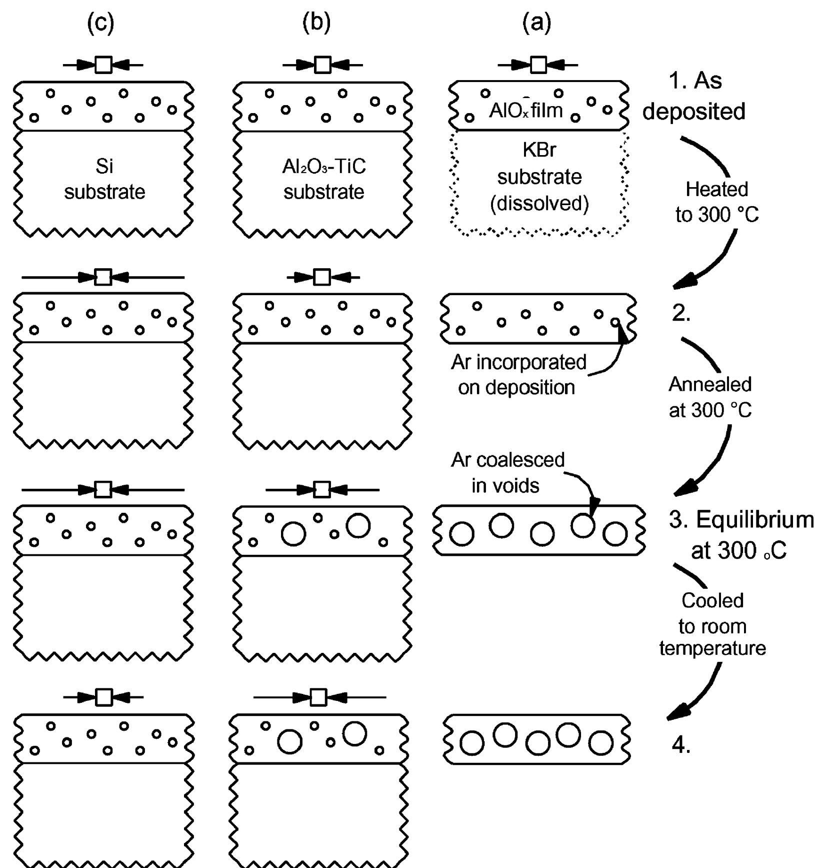

Figure 9 Schematic diagrams representing changes in the configuration of retained Ar in PVD AlO_x films during annealing with various constraints: (a) no substrate, no constraint, dissolved Ar coalesces with free expansion; (b) AlTiC substrate, initial mild compressive constraint, complete coalescence impeded by build-up of compressive stress on exsolution; (c) Si substrate, large compressive constraint, no exsolution and coalescence.

equilibrium by "precipitating" Ar out of solution into voids. In this case, however, the consequent imposed expansion is constrained by the substrate, leading to the development of a greater compressive stress, which slows the precipitation process. This irreversible path is indicated on the diagram by the (diagonal) dashed line. Eventually the combined unprecipitated Ar concentration and stress state reach the equilibrium values of $C_{\rm Ar} > 1$ appropriate to $T = 300°C$ and $\sigma_{\rm f} \sim -90$ MPa and the precipitation and expansion processes halt. On rapid cooling to room temperature from this state the tensile stress associated with the CTE mismatch reverses (short horizontal solid line) adding to the the irreversible compressive stress change acquired during the anneal, leading to a large compressive stress hysteresis The film remains metastably trapped in this state, which is indicated on the diagram by the boxed symbol AlTiC.

The above discussion suggests that only for a few circumstances are PVD AlO_x films in thermodynamic—chemical and mechanical—equilibrium. In addition, the films assume a range of equilibrium states depending on the substrate and the consequent CTE mismatch. The CTE mismatch determines the stress state of the film which couples to the volume change associated with Ar exsolution, thereby coupling chemical and mechanical effects, leading to a range of possible isothermal equilibria. This is made clear in Fig. 9, in which all three film-substrate systems are in very different equilibrium configurations at the end of the anneal, state 3, and arrived and departed from these configurations in different ways: The no substrate system arrived there by purely chemical changes from the start of the anneal, state 2, and remained there on cooling to room temperature, state 4; the Si substrate system arrived there by purely mechanical changes on the heating from room temperature, state 1 to state 2, and returned to the initial non-equilibrium condition on cooling; the AlTiC substrate system arrived there by a coupled combination of chemical and mechanical changes during the anneal, state 2 to state 3, and moved to a different non-equilibrium configuration on cooling.

Temperature during annealing or thermal cycling therefore affects the thermal stability of PVD AlO_x films in two ways; by setting the stress state associated with CTE mismatch with a substrate and by determining the kinetics of coupled chemo-mechanical changes of state of incorporated sputtering gases. The actual stress state of a film thus depends critically on the substrate and the thermal history. Hence during device processing and use, the mechanical responses and related reliability of such films, which depend critically on the stress state, will depend on the thermal history. Part II of this series examines the mechanical properties of PVD AlO_x films and their dependence on the stress state.

6. Summary

The thermal stability of non-reactive sputtered AlO_x films of varying thickness on Al_2O_3-TiC and Si substrates deposited at two different substrate biases was examined. The films were deposited in compression and film stress measurements on thermal cycling identified an irreversible increase in compressive stress during cycling and annealing at elevated temperatures. The room temperature deposition stress, about −45 MPa, and thermo-mechanical response were independent of film thickness (between 5 and 50 μm) and substrate bias during deposition. Conversely, the thermo-mechanical response was not independent of substrate. Whereas AlO_x deposited on AlTiC substrates irreversibly developed about 75 MPa greater compression on thermal cycling, that on Si substrates exhibited negligible hysteresis and developed tensile stress during annealing. The difference in behaviour was as interpreted as a dependence of the solubility of retained sputtering gas on the absolute magnitude of stress during the anneal, a quantity affected by the CTE mis-match with the substrate. There exists some equilibrium magnitude of film stress at the anneal temperature that drives stress development and controls both the magnitude and sign of nonlinear stress development.

References

1. R. S. NOWICKI, *J. Vac. Sci. Technol.* **14** (1977) 127.
2. K. G. KREIDER, *ibid.* A **4** (1986) 2618.
3. J. C. GODEFROY, C. GAGEANT, D. FRANCOIS and M. PORTAT, *ibid.* A **5** (1987) 2917.
4. P. VUORISTO, T. MANTYLA and P. KETTUNEN, *J. Mater. Sci.* **27** (1992) 4985.
5. J. P. LEHAN, R. B. SARGENT and R. E. KLINGER, *J. Vac. Sci. Technol.* A **10** (1992) 3401.
6. K. K. SHIH and D. B. DOVE, *ibid.* A **12** (1994) 321.
7. C. A. ROSS and R. MALMHALL, in Proceedings of the 3rd International Symposium on Magnetic Materials, Processes and Devices, edited by L. T. Romankiw and D. A. Herman (The Electrochemical Society, Pennington NJ, 1994) p. 165.
8. C. S. BHATIA, G. GUTHMILLER and A. M. SPOOL, *J. Vac. Sci. Technol.* A **7** (1989) 1298.
9. R. A. GARDNER, P. J. PETERSON and T. N. KENNEDY, *ibid.* **14** (1977) 1139.
10. P. VUORISTO, T. MANTYLA and P. KETTUNEN, *Thin Solid Films* **204** (1991) 297.
11. C. A. ROSS, *J. Vac. Sci. Technol.* A **14** (1996) 2511.
12. K. CHRISTOVA and A. SZEKERES, *Semicond. Sci. Technol.* **6** (1991) 748.
13. T. HANADA, H. FURUYA, S. TANABE and N. SOGA, *J. Non-Cryst. Solids* **152** (1993) 188.
14. G. G. STONEY, *Proc. R. Soc. Lond.* **A82** (1909) 172.
15. Product Bulletin, Minnesota Mining and Manufacturing Company, St. Paul, MN, 1987.
16. W. A. BRANTLEY, *J. Appl. Phys.* **44** (1973) 534.
17. T. F. RETAJCZYK, JR. and A. K. SINHA, *Appl. Phys. Lett.* **36** (1980) 161.
18. S. H. LAU, S. HUANG and A. KOO, *Semicond. Intern.* **23** (2000) 239.
19. J. THURN and R. F. COOK, *J. Appl. Phys.* **91** (2002) 1988.
20. P. A. FLINN, A. S. MACK, P. R. BESSER and T. N. MARIEB, *MRS Bull.* **18** (1993) 26.
21. L. DOUCET and G. CARLOTTI, "Mat. Res. Soc. Symp. Proc." (MRS, Pittsburgh PA, 1995) Vol. 356, p. 215.
22. L. A. CHOW, B. DUNN and K. N. TU, *J. Appl. Phys.* **87** (2000) 7788.
23. C. FITZ, A. KOLITSCH and W. FUKAREK, *Thin Solid Films* **389** (2001) 173.
24. R. A. SWALIN, "Thermodynamics of Solids," 2nd ed. (John Wiley and Sons, 1972) p. 178.

Received 4 November 2003
and accepted 6 April 2004